Journal of
Tissue Science & Engineering
ISSN: 2157-7552

Sawyer et al., J Tissue Sci Eng 2016, 7:2
DOI: 10.4172/2157-7552.1000173

Research Article Open Access

Behavior of Encapsulated Saos-2 Cells within Gelatin Methacrylate Hydrogels

Stephen W Sawyer[1], Megan E Oest[2], Bryan S Margulies[2] and Pranav Soman[1]*

[1]*Department of Biomedical and Chemical Engineering, Syracuse Biomaterials Institute, Syracuse University, Syracuse, NY, USA*
[2]*Department of Orthopedic Surgery, Institute for Human Performance, SUNY Upstate Medical University, Syracuse, NY, USA*

Abstract

The field of tissue engineering is still seeking a viable substitute to repair and replace damaged bone using a combination of porous implants, biochemical factors, and relevant cell types. While progress in this field has been made, current engineered solutions have not been able to mimic the architectural and biological requirements needed to provide a complete solution. In this work, bone-like human osteosarcoma cells were encapsulated inside gelatin methacrylate (GelMA) hydrogels of three different weight/volume (w/v) concentrations and stimulated to form mineral in order to determine the relationship between both bone formation and cellular activity with matrix stiffness. Distinct differences between cell morphology and mineral formation were found within the three types of hydrogels. Softer, less dense constructs were shown to provide a more cell friendly microenvironment that promoted dispersed mineral formation while stiffer, dense constructs provided a more structured environment for uniform bone-mineral formation. Additionally, while cells were able to function in all three types of hydrogels, cells in the softer GelMA constructs were shown to grow in large colonies within the gelatin matrix while cells in the stiffer GelMA constructs tended to aggregate and grow along the construct peripheries.

Keywords: Hydrogel; Gelatin methacrylate; Saos-2 cells; Mineralization; Cell-encapsulation

Introduction

Bone has emerged as the second most transplanted tissue in the world with forecasted revenue of $6.6 billion by 2020 in the United States alone [1,2]. While clinical grafts are used in many reparative orthopedic procedures, they often fail due to graft necrosis and lack of integration with host tissue [3,4]. Due to the limited success of such grafts, numerous alternative solutions to repairing and regenerating bone have been proposed that consist of combinations of different types of porous osteoconductive biomaterials, osteoinductive growth factors and osteogenic cells [5-8]. However, no single option has emerged as a complete engineered solution. When creating a proper bone tissue substitute, several variables need to be taken into account: the scale of the implant needs to be optimized for proper vascularization and nutrient distribution, the base material must be biocompatible and biodegradable in ways that promote high cell viability and natural tissue growth, and the mechanical support of the implant should be suitable for proper weight bearing applications [2,7-11]. Current tissue engineering strategies have not been able to address all of the aforementioned variables for an organ as intricate as bone. Traditionally, bone tissue engineering has adopted the strategy of machining scaffolds that provide structural support followed by the seeding of relevant cells onto the construct post-manufacturing. Although the exclusion of living cells during manufacturing gives the flexibility of using a variety of fabrication techniques needed to make intricate tissue substitutes, the cell seeding approach relies on the passive ability of cells to infiltrate the interiors of the 3D scaffold and often results in inadequate cell dispersion and cellular densities. To address this limitation, another manufacturing approach involving cell encapsulation within a soft biomaterial has also been widely explored. Cell encapsulation generally utilizes either synthetic or naturally derived hydrogels and includes the incorporation of living cells into a hydrated matrix during fabrication, thus allowing for the precise control over the cellular density and distribution within a soft 3D construct [12-15].

Although cell encapsulation is an appealing approach for the incorporation of relevant cells and growth factors into a bone tissue substitute, several issues need to be addressed. Not only is it important to know how the hydrogel properties influence the viability and function of encapsulated osteoblastic cells, it is important to understand how soft hydrated matrices influence bone mineral formation. Furthermore, the soft cell-laden hydrogels need to be integrated within a protective, structural frame in order to realize the goal of developing a clinically relevant biomimetic construct for bone tissue engineering. In this current study, we focus on how encapsulated cells interact within the hydrated microenvironment of a soft bone tissue substitute. To this end, we encapsulate bone-like human osteosarcoma cells (Saos-2) inside GelMA hydrogels of varying weight/volume (w/v) concentrations and stimulate them to form mineral in order to determine the relationship between bone formation and hydrogel stiffness.

Materials and Methods

Gelatin methacrylate pre-polymer solution preparation: Gelatin methacrylate (GelMA) macromer was synthesized using a previously reported protocol to serve as the base hydrogel matrix for cellular encapsulation [16,17]. Briefly, porcine skin gelatin (Sigma Aldrich) was mixed at 10% (w/v) in phosphate buffered saline (PBS, Thermo Fisher Scientific), stirred at 45°C, mixed with methacrylic anhydride and stirred for 3 h. After stirring, the solution was dialyzing against distilled water for one week at 40°C, freeze-dried, and stored at -80°C until needed. For cell encapsulation experiments, three different GelMA pre-polymer solutions (7, 10 and 15% w/v) were created by combining the

***Corresponding author:** Pranav Soman, Department of Biomedical and Chemical Engineering, Syracuse Biomaterials Institute, Syracuse University, Syracuse, NY, USA, Tel: 315-443-9322; E-mail: psoman@syr.edu

Received July 06, 2016; **Accepted** July 26, 2016; **Published** July 31, 2016

Citation: Sawyer SW, Oest ME, Margulies BS, Soman P (2016) Behavior of Encapsulated Saos-2 Cells within Gelatin Methacrylate Hydrogels. J Tissue Sci Eng 7: 173. doi:10.4172/2157-7552.1000173

freeze-dried GelMA macromer with various amounts of PBS and 0.25% UV photoinitiator Irgacure 2959 (Specialty Chemicals, Switzerland). The pre-polymer solutions were sterile filtered and stored at 2°C in autoclaved Pyrex bottles (Corning) wrapped with tin foil. Pre-polymer solutions below 7% were not used as they were not capable of being photo-cured while pre-polymer solution above 15% were not capable of being properly dissolved and sterile filtered.

Saos-2 culture and encapsulation: We employed human osteosarcoma cells (Saos-2; ATCC) transfected with a commercially available green fluorescent protein (GFP) lentivirus (Santa Cruz Biotechnology) as analogues for osteoblasts since they are a robust cell line commonly used in the initial stages of new bone defect models [18]. The GFP tagged Saos-2 cells were cultured in Dulbecco's Modification of Eagle's Media (DMEM; Life Technologies) supplemented with 10% fetal bovine serum (v/v) (FBS lot G12102; Atlanta Biologicals), 1% penicillin-streptomycin (Life Technologies) and 1% GlutaMAX (Life Technologies). Cells were passaged using standardized protocols with 0.25% trypsin-EDTA (Life Technologies) and maintained at conditions of 37°C with 5% CO_2. Cells were encapsulated in GelMA matrices of varying densities by mixing 20 µL of a stock cell solution containing approximately 3750 cells/µL with 130 µL of 7%, 10% or 15% GelMA pre-polymer solution (w/v). The cell/GelMA solution was pipetted drop-wise into 5 mL of autoclaved vegetable oil and UV cured for 1 min with an intensity of 5 mW/cm^2 using a Hamamatsu LED Controller (Hamamatsu C11924-511; Hamamatsu Photonics K.K., Japan), taking advantage of an oil emersion based surface tension technique for cell encapsulation (Figure 1A) [19]. The solidified GelMA hydrogels containing encapsulated cells were then washed five times with 5 mL of sterile PBS, transferred into 2 mL of supplemented DMEM, and cultured as previously reported. Media was exchanged on each construct every 2 to 3 days until being fixed with 2% paraformaldehyde (Sigma) in PBS.

Osteosarcoma mineralization: Saos-2 cells were encapsulated and cultured as previously mentioned for specific durations of time before being chemically stimulated to produce mineral. Specifically, Saos-2 cells were encapsulated at approximately 75,000 cells per construct and allowed to grow for either 7 days (for histological staining assays) or 2 weeks (for microCT) before being chemically stimulated with an induction media. The induction media consisted of DMEM containing 10% FBS and 1% PSG supplemented with 0.1 µM dexamethasone (Sigma Aldrich), 25 µg/mL L-ascorbic acid-2-phosphate (AA2P; Sigma Aldrich), and an increasing regiment of β-glycerophosphate (BGP; Sigma Aldrich) [18]. The BGP regimen included one media change with 5 mM BGP, followed by one media change with 10mM BGP and all subsequent media changes containing 20 mM BGP. Once the specific time points for each experiment were reached, the samples were fixed in a 2% paraformaldehyde solution and cryo-protected with a 30% sucrose solution for both micro-computed tomographies imaging and sectioning.

Histochemical analysis, Live/Dead staining, and image processing: All encapsulated samples were fixed at the appropriate time points in a 2% formaldehyde solution. Chemically stimulated samples were cryo-protected with a 30% sucrose solution in PBS for both micro-computed tomography imaging and sectioning, while non-stimulated samples were decalcified and cryo-protected using a 14% ethylenediaminetetraacetic acid (EDTA; Sigma) and 30% sucrose solution in PBS. Samples to be sectioned were embedded in Tissue Freezing Medium Blue (TFMTM; Electron Microscopy Sciences), snap frozen using liquid nitrogen and sectioned into 10 µm slices using a Leica CM3050 cryostat (Leica Biosystems, Germany). Following sectioning, non-chemically stimulated samples to be stained for f-actin were treated with 0.1 M sodium citrate buffer solution pH 6.0, washed with PBS, and stained with Alexa Fluor 568 Phalloidin (1:100 dilution; Life Technologies). Nuclei were counterstained with 2.5 µg/mL 4', 6-diamidino-2-phenylindole (DAPI) (1:50 dilution; Life Technologies) in PBS. Following sectioning, all chemically stimulated samples to be analyzed for mineral were stained with 40 mM alizarin red S pH 4.2 (1:100 dilution; Sigma Aldrich) and counterstained with 2.5 µg/mL DAPI (1:50 dilution) in PBS. The viability of cells was analyzed using a Live/Dead assay. To evaluate cell viability, all three different types of hydrogels containing encapsulated cells were placed in media containing calcein-AM (1:2000 dilution; Life Technologies) and

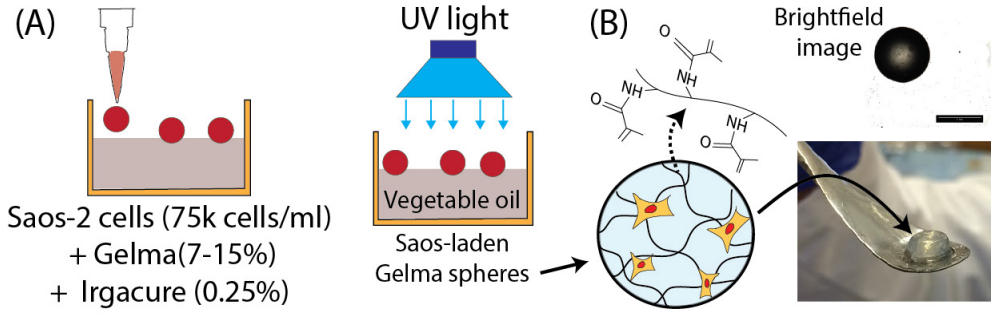

(C)

% GelMA (w/v)	Compression Modulus (kPa)	Mass Swelling	Storage Modulus (Pa)
7	14.78 +/- 2.14	0.94 +/- 0.011	1055
10	24.95 +/- 4.99	0.91 +/- 7.27E-04	1844
15	63.73 +/- 7.78	0.83 +/- 7.51E-03	3098

Figure 1: Cellular encapsulation schematic. **(A)** Schematic of surface tension encapsulation technique. 75,000 Saos-2 cells in 20 µl aliquots were combined with 130 l of pre-polymer solution containing. 25% photo initiator and pipetted drop wise into a bed of vegetable oil. UV light was cast onto the hydrogel drops for one minute to cure before being rinsed with PBS and transferred into incubation media. **(B)** Cured hydrogel spheres containing encapsulated cells resembled disc like structures with dimensions approaching 6 mm × 6 mm × 4 mm (scale bar=5 mm). **(C)** Mechanical data of various GelMA (w/v) concentrations modified from previous work [17].

ethidium homodimer (1:500 dilution; Life Technologies) after 5 days of growth and incubated at 37°C for 1 h. Raw .tiff images were taken for all sectioned samples using an epifluorescence equipped Nikon Eclipse E-400 microscope (Nikon Corporation). All reported images were processed linearly for brightness and contrast using Adobe Photoshop CC 2015 (Adobe Systems Inc.). Once adjusted for brightness and contrast, images were converted to gray scale and subsequently overlaid to produce published images.

Micro-computed tomography: Chemically stimulated samples were fixed in a 2% formaldehyde solution and subsequently cryo-protected with a 30% sucrose solution for micro-computed tomography imaging and sectioning. A Scanco micro-CT 40 (Scanco Medical) was used to image and quantify mineral formation in chemically stimulated samples. Samples were placed in groups of 3 inside gauze packed micro-CT canisters and kept hydrated with 2% formaldehyde solution during imaging.

Quantitative values and statistical analysis: All quantitative values, with the exception of micro-computed tomography values, were obtained using open-source ImageJ (NIH) software. Retrieved data was entered manually into Microsoft Excel (Microsoft Corporation) where values were reported as means ± standard deviation. One-way ANOVA was performed using Microsoft Excel data pack. P-values <0.05 were considered statistically significant.

Results

Formation of cell-laden hydrogels

In order to determine how osteoblast like cells behaved while encapsulated within a soft gelatin matrix, 75,000 Saos-2 cells were mixed with three different concentrations of GelMA prepolymer solution (7%, 10% and 15% w/v), pipetted into an oil bath to form hydrated beads, and UV cured for 1 min (Figure 1A). Free radicals released from the photoinitiator (Irgacure 2959) in the pre-polymer solution caused the covalent binding of acrylate groups during the UV exposure, thereby crosslinking GelMA drops (~ 6 mm × 6 mm × 4 mm) (Figure 1B). This technique utilized the surface tension between aqueous GelMA solution and vegetable oil to crosslink GelMA drops at the air-GelMA-oil interface, and provided an easy-to-use approach with high degree of reproducibility [19]. A relatively low seeding density was used in order to maximize cell-matrix interactions within the three different types of hydrogels and the volume of the drops was specifically chosen to mimic murine bone defects.

Viability of encapsulated cells

The size of the hydrogel drop was designed to maximize cell-matrix interactions in a porous space that mimicked a murine bone defect. Viability was quantified 5 days after encapsulation using ethidium homodimer (dead cells=red staining) versus calcein-AM (live cells=green staining) (Figure 2A). It was found that there was an

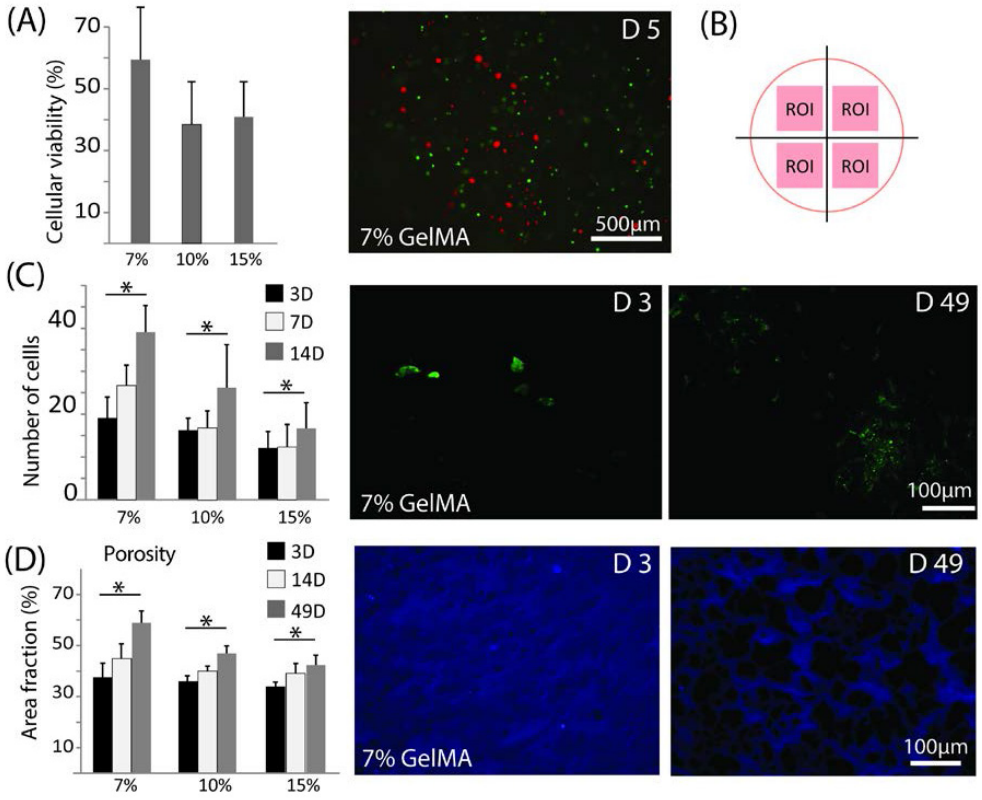

Figure 2: Cellular viability and activity within degradable hydrogel scaffolds of different stiffness. **(A)** Cells were grown within hydrogel constructs for 5 days and analyzed for cellular viability using calcein-AM (live=green) and ethidium homodimer (dead=red). Fluorescent images of live/dead cells show live and dead cells throughout the entire scaffold. **(B)** Representative schematic of the region of interest used to standardize measurements between fixed and sectioned histological samples. Areas between the center of the slices and the peripheries were used due to sectioning artifacts. **(C)** Cells stained with DAPI were counted in the ROI of histological slices for 3 day, 7 day and 14 day time points. Increases in cellular population over time within the hydrogels were evident in all samples at all timepoints (n=3; *=p<0.05). **(C)** Saos-2 cells tagged with green fluorescent protein (GFP) showed activity in all samples well over one month after encapsulation (scale bar=100 µm). **(D)** Fluorescence in histological samples due to DAPI staining allowed for apparent porosity of hydrogels containing encapsulated cells to be measured for 3 day, 14 day and 49 day time points. Blue coloring represents GelMA staining while black coloring represents apparent void space. All gels degraded significantly over time (n=3; *=p<0.05; scale bar=100 µm).

apparent higher viability in the softer 7% hydrogels with approximately 60% live as opposed to only 40% live in both the 10% and 15% gels. However, since cells are required to be within 200-300 μm of a nutrient supply in order to properly function *in vivo* and due to inherent diffusion limitations in constructs many millimeters in size, low cell viability was observed. In order to determine how cells behaved within the hydrogel matrices at various stages of growth, histological sectioning was performed. Accordingly, the GelMA drops were fixed in 2% paraformaldehyde and cryosectioned into 10 μm slices to allow for imaging. A specific region of interest (ROI) was chosen to standardize measurements between samples (Figure 2B). Specifically, the ROI used in all analysis was determined to be the area between the center of the sectioned slices and the corresponding slice periphery.

Due to expected nutrient diffusion limitations within the stiffer hydrogels, it was necessary to quantify cell number in the sectioned ROIs at specific time points to determine cell migration patterns. To analyze whether cells were forming colonies inside the bulk material or simply migrating out of the constructs, cells were counted in the ROIs for each of the three types of hydrogels at 3 day, 7 day and 14 day time points by staining fixed slices with DAPI (nuclei) (Figure 2C Left). More cells were counted, on average, in the ROIs of the 7% gels at all-time points and decreased as the gels became stiffer. For the 3 day time point, 19 cells on average were observed in the 7% constructs while only 12 cells were counted in the 15% constructs. Additionally, over time the number of cells within the ROI of the 7% gels increased at a higher rate than those in the 15% gels, with 39 cells on average appearing in the 7% and only 17 cells appearing in the 15%. This represented an approximately 100% increase in the amount of cells in the ROI of the soft gel with only a 41% increase in the stiffer gel.

Cells encapsulated within GelMA spheres were transfected with GFP in order to determine spatial cell location inside the scaffolds prior to fixation, as well as inherent cellular activity at all stages of growth. At each specified time point, fixed and sectioned samples were imaged for green emissions to ensure that counted cells were still active. In addition to the standard 3 day, 7 day and 14 day time points, cells were imaged inside of the ROIs well over 1 month after the initial photo curing to show long term activity (Figure 2C Right).

As a result of DAPI nuclei staining, the GelMA matrices of all three types of hydrogels fluoresced when exposed to UV light, thereby allowing for construct degradation to be measured. Constructs were fixed and stained with DAPI at 3 day, 14 day and 49 day time points in order to determine if a quantifiable relationship existed between bulk matrix degradation and hydrogel stiffness (Figure 2D). In general, softer hydrogels showed higher porosities (defined as void area fraction within a 10 μm slice) than stiffer hydrogels at all-time points. Compared to the stiffest 15% hydrogels, 7% gels were 4% more porous at 3 days, 7% more porous at 14 days and 16% more porous at 49 days. Additionally, it was shown that stiffer gels degraded slower over time, with 7% gels increasing in porosity by 21% from 3 to 49 days, compared to an 11% increase in 10% gels and a 9% increase in 15% gels.

Cellular morphology

In addition to showing cell migratory differences throughout the three different hydrogel constructs, cell morphology was cataloged at different time points to determine if matrix stiffness had an effect on cellular growth. Cell morphology was determined in the ROI for each of the three types of gels at 3 day, 7 day and 14 day time-points by staining fixed construct slices with DAPI (nuclei) and phalloidin (f-actin). At early time points, cell morphology appeared similar in the 7%, 10% and 15% gels, but changed dramatically at the later time points. At later time points, cells within the ROI in the softer gels formed large, defined clusters while cells in the 10% and 15% gels formed either limited or no clusters. Representative images of each type of construct indicate significant differences between cellular aggregations and morphology between the 7%, 10% and 15% samples (Figure 3A Top). This observation is evident in the high-resolution photographs at the 14D time point (Figure 3A Bottom).

The aggregate nucleus diameter and area of encapsulated cells, as well as the aggregate lacunae diameter and area of encapsulated cells, were quantified in order to highlight the differences between how cell colonies grew within the bulk matrix of the three different hydrogels (Figure 3B). The aggregate area and diameter of nuclei stained with DAPI were rather consistent for all different gels at each of the three time points, except for numerous large clusters of nuclei that were predominately observed in the softer 7% gels after 14 days of culture. Synonymously, the aggregate lacunae area and diameter were similar in all scaffolds at each stage of growth except for the large clusters of cells that formed intricate lacunae after 14 days in the soft 7% gels.

Mineral deposition

To better examine the potential effects of matrix stiffness on osteogenesis, Alizarin red S staining was used to identify the presence of deposited calcium in chemically stimulated hydrogels. Cells were stimulated to produce mineral 7 days after encapsulation and were subsequently grown for an additional 2 weeks in osteogenic media in order to determine what effect hydrogel stiffness had on bone nodule formation. Alizarin red and DAPI counterstain were used to visualize fixed samples for mineral (Figure 4A) and mineral content and mineral area within the ROI was quantified (Figure 4C). Consistent with previous results, the total area fraction of mineral within the ROI was greater by 3 fold in the ROI of softer 7% gels than in the stiffer 15% gels, while mineral clusters in the ROI of softer hydrogels had areas 3.5 fold greater than those in stiffer gels.

A different group of samples were grown for 2 weeks in order to mimic the 14 day culture period used in the cellular morphology studies and were subsequently stimulated in osteogenic media for an additional 14 days. After four weeks, samples were fixed and scanned via microCT to determine total bone mineral content (Figures 4B and 4C). Softer 7% hydrogels showed indiscrete mineral formation throughout the entire construct while stiffer 15% gels showed concentrated mineral formation at the peripheries. Total mineral density appeared to be similar in both the 7% and 15% samples with 0.053 mg HA and 0.058 mg HA, respectively.

Discussion

As compared to conventional studies performed on non-physiological 2-D substrates, Saos-2-laden GelMA hydrogels provide a more realistic 3-D environment with which to study bone regeneration [20,21]. Although human osteosarcoma Saos-2 cells do not completely represent the response of primary human osteoblasts, Saos-2 do serve as a robust, model cell line capable of allowing for the assessment of the biocompatibility and differentiating potential of the GelMA matrix. As such, the results from this work indicate that the stiffness of GelMA plays a vital role in encapsulated cell viability, morphology, and function.

UV cross-linking of photopolymers have several advantages over both chemical and ionic (physical) crosslinking strategies. UV cross-linking allows for easy tuning of material properties, eliminates the

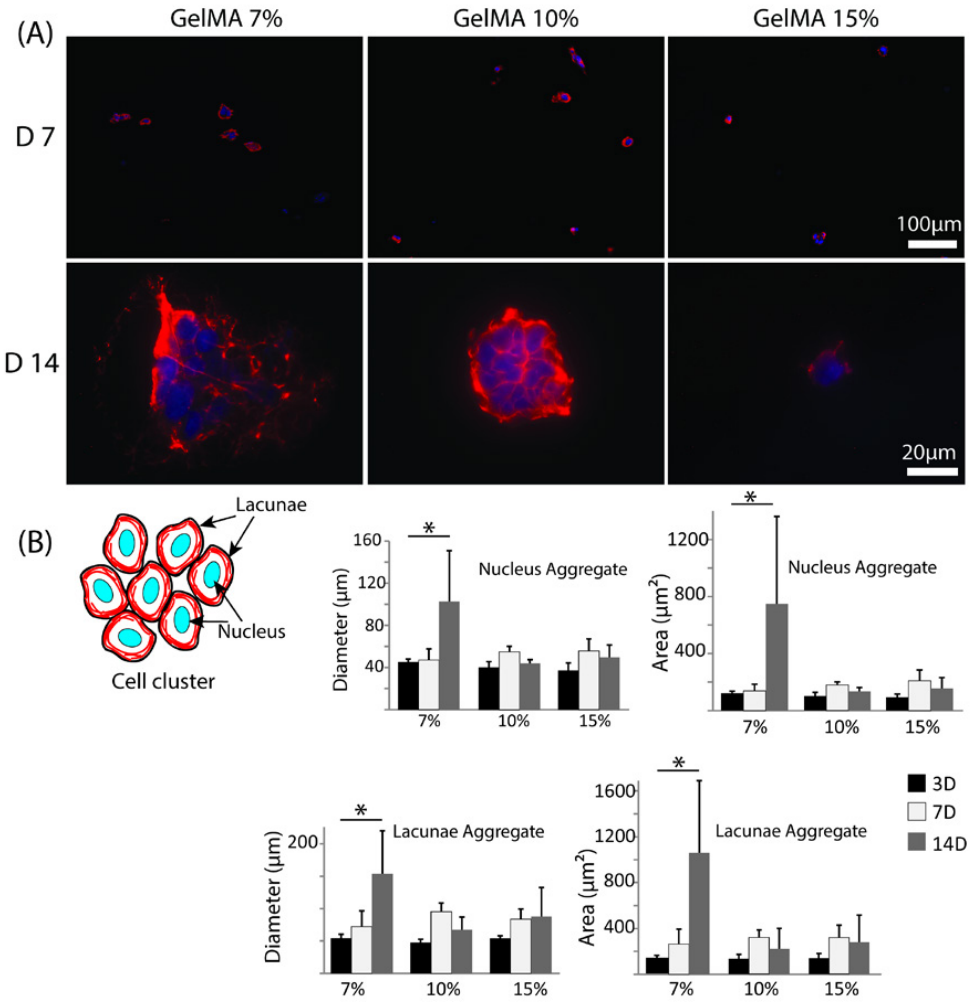

Figure 3: Nuclear and cytoskeleton staining of encapsulated Saos-2 cells. **(A)** Cells were grown within hydrogel constructs for either 3, 7 or 14 days, fixed, sectioned, and stained for f-actin (red=phalloidin) and counterstained for nuclei (blue=DAPI). Representative pictures at 7 days (scale bar=100 µm) and 14 days (high resolution; scale bar=20 µm) show distinct morphological differences in the ROI of samples of different stiffness at all-time points. **(B)** Histological samples stained with phalloidin and counterstained with DAPI were analyzed for morphological differences in the nuclei and lacunae at 3 day, 7 day and 14 day time points. Measurements showed significant differences in aggregate nuclear diameters and areas, as well as aggregate lacunae diameters and areas, for softer hydrogels over time (n=3; *=p<0.05).

need for organic solvents and provides short reaction times. One recent study reported the encapsulation of human mesenchymal stem cells within a synthetic hydrogel containing Irgacure 2959 photoinitiator and demonstrated excellent cellular viability 14 days after UV crosslinking for varying curing times [22]. Specifically, UV light (100 W/365 nm) was exposed to hMSC-laden hydrogels for times varying between 2.5 min and 10 min and DNA damage was not detected when exposure time was kept around 2.5 min. Other studies, which used similar UV crosslinking techniques for 2-3 min, also demonstrated no significant changes or damage to the cells as a result of UV exposure [23]. In our study, we only use an exposure time of 1 min, much lower than the reported times causing observable DNA damage.

Recent work with UV-cross-linkable hydrogels containing living cells has shown success in an *in vivo* setting. Specifically, N-methacryloyl chitosan hydrogels mixed with living cells was demonstrated to undergo rapid transdermal crosslinking *in vivo* within 60 s through minimally invasive clinical surgery. Histological analysis revealed that low-dose UV irradiation did not induce skin injury and the acute inflammatory response disappeared after only 7 days [24]. Another study showed that encapsulated bone marrow-derived mesenchymal stem cells in UV crosslinked GelMA hydrogels demonstrated enhanced osteogenesis *in vivo* with significant mineralization [25]. In yet another study, GelMA hydrogels containing multipotent stromal cells within an ectopic rat model was used to engineer endochondral bone [26].

As mentioned previously, low cellular viability of encapsulated osteosarcomas was expected since cells are required to be within 200-300 µm of a nutrient supply in order to properly function *in vivo*. Due to the larger size of our cell-laden hydrogels and inherent diffusion limitations associated with dense constructs, viabilities ranging from 40 to 60 percent were normal. In a similar study, Saos-2 cells were encapsulated within sodium-alginate drops of only 1mm in diameter and were found to survive at higher rates as compared to the GelMA drops used in this study, further emphasizing the role media diffusion plays in maintaining high levels of cellular viability [27].

The observed cell count differences in the ROIs of the three different gels suggested that cells were migrating outside of the denser constructs due to poor nutrient diffusion. This result was in line with a recent study where it was shown that the cellular viability of encapsulated

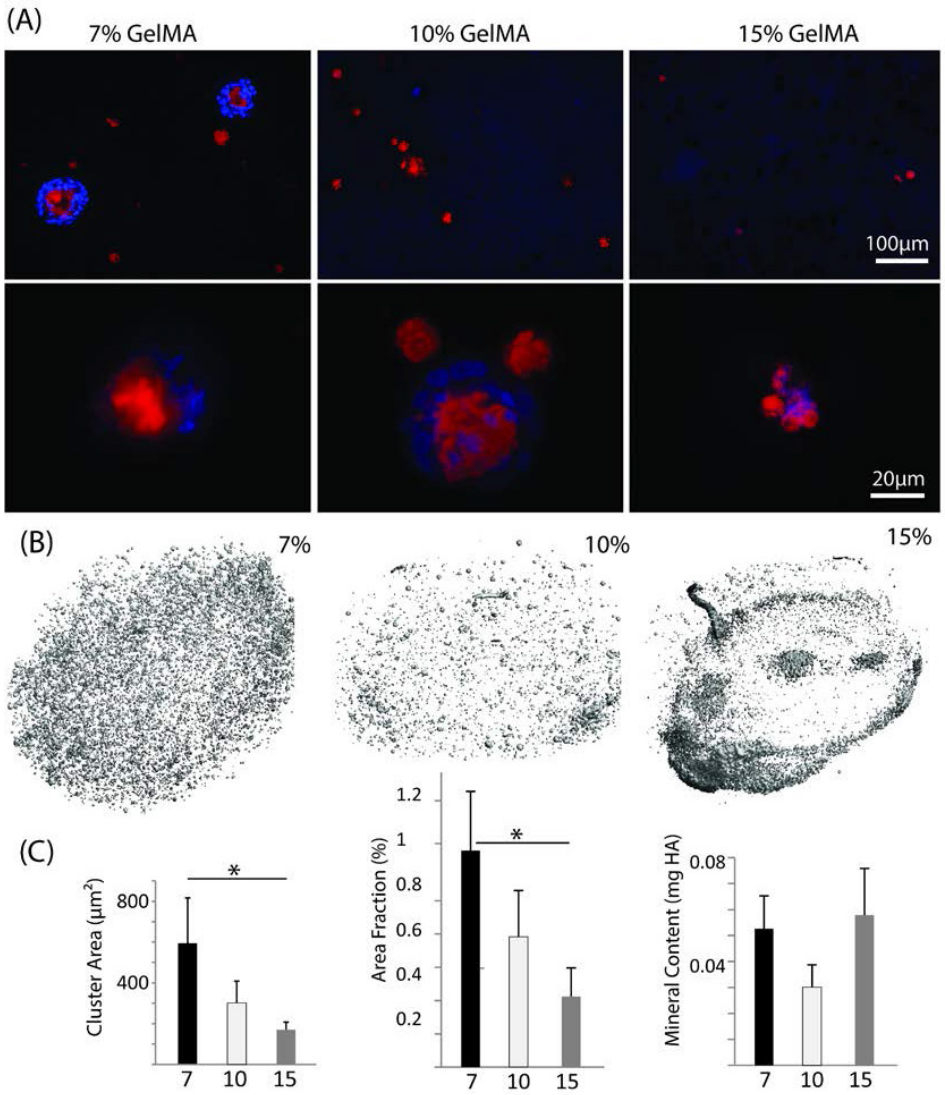

Figure 4: Mineralization and microCT of encapsulated Saos-2 cells. **(A)** Cells were grown within hydrogel constructs for 7 days and were subsequently placed in osteogenic media for an additional 14 days. Constructs were fixed, sectioned, stained for mineral deposition (red=alizarin red S) and counterstained for nuclei (blue=DAPI). Representative pictures for all samples show distinct difference in the mineral located within the ROI for different gel stiffness (top scale bar=100 µm; bottom scale bar=20 µm). **(B)** Cells were grown within hydrogel constructs for 14 days and were subsequently placed in osteogenic media for an additional 14 days. Samples were analyzed via microCT for total mineral within the constructs of different stiffness. **(C)** Histological samples stained with alizarin red S and counterstained with DAPI were analyzed for mineral cluster area and area fraction of mineral coverage within the ROI and showed significant differences for implants of varying moduli (n=2; *=p<0.05). MicroCT scans were analyzed for total mineral throughout the constructs and showed no significant differences between implants of varying moduli (n=3).

mesenchymal stem cells (MSCs) inside the matrix of porous gelatin constructs increased as porosity increased [28]. Additionally, the observation that cells within the ROIs of the more porous matrices were able to form larger clusters further suggested that cells within the softer gels remained active in the bulk material while cells in the stiffer gels migrated towards the peripheries. Furthermore, the ability of cells within the 7% and 10% hydrogels to form defined cell colonies was consistent with existing literature detailing how cells behave while encapsulated in soft material. One recent study used sub-millimeter sized beads to encapsulate MG-63 osteosarcoma cells within gelatin-modified alginate (AlGel) hydrogels [29] and showed that the clusters of cells that formed within the AlGel had several protrusions with lengths of approximately 30 µm extending between colonies. Similar phenomena have also been observed within encapsulated hematopoetic stem cells [30] and human embryonic stem cells [31].

In this work, we used GelMA, a collagen derivative, as our soft component since it has tailorable mechanical properties, is able to be chemically modified with various peptides, is biodegradable, and has crosslinked environments similar to the natural extracellular matrix (ECM). Although stiffer GelMA matrices showed less cellular activity near the center of the construct, cells were still metabolically active and capable of surviving. Additionally, since there were no significant differences between the amounts of mineral produced in the 7% constructs versus the 15% constructs, it could be suggested that the encapsulated cells in the harder scaffolds migrated towards the periphery in order to uniformly encase the structure. Based on these observations, it is plausible to suggest that properly vascularized hydrogels of increased stiffness could encourage osteogenic cells to create mineral in a consistent, ordered fashion.

Conclusion

This work showcases the advantages of using a gelatin-based porous hydrogel for bone tissue engineering. By understanding how the bone-like cells function within hydrogels of different stiffness, it may be possible to capitalize on this knowledge and design more complex structures capable of directed bone formation.

Acknowledgement

We would like to thank Shihao Yang for his assistance in synthesizing GelMA macromer and analyzing data, as well as Sean DeBoyace for his help in culturing cells. This work was supported by the Soft Interfaces Integrative Graduate Education and Research Traineeship (IGERT) DMR-DGE- 1068780 at Syracuse University and funded by the National Science Foundation (NSF).

References

1. Liu Y, Lim J, Teoh SH (2013) Review: Development of clinically relevant scaffolds for vascularised bone tissue engineering. Biotechnology advances 31: 688-705.
2. Amini AR, Laurencin CT, Nukavarapu SP (2012) Bone tissue engineering: Recent advances and challenges. Crit Rev Biomed Eng 40: 363-408.
3. Eastlack RK, Garfin SR, Brown CR, Meyer SC (2014) Osteocel plus cellular allograft in anterior cervical discectomy and fusion: Evaluation of clinical and radiographic outcomes from a prospective multicenter study. Spine 39: E1331-E7.
4. Deyo RA, Ching A, Matsen L, Martin BI, Kreuter W, et al. (2012) Use of bone morphogenetic proteins in spinal fusion surgery for older adults with lumbar stenosis: Trends, complications, repeat surgery and charges. Spine 37: 222-230.
5. Griffith LG, Naughton G (2002) Tissue engineering--current challenges and expanding opportunities. Science 295: 1009-1014.
6. Loh QL, Choong C (2013) Three-dimensional scaffolds for tissue engineering applications: Role of porosity and pore size. Tissue Eng Part B Rev 19: 485-502.
7. Burg KJ, Porter S, Kellam JF (2000) Biomaterial developments for bone tissue engineering. Biomaterials 21: 2347-2359.
8. Reichert JC, Hutmacher DW (2011) Bone tissue engineering. Tissue Engineering, Springer 431-456.
9. Bose S, Vahabzadeh S, Bandyopadhyay A (2013) Bone tissue engineering using 3D printing. Materials Today16: 496-504.
10. Stevens MM (2008) Biomaterials for bone tissue engineering. Materials today 11: 18-25.
11. Hutmacher DW (2001) Scaffold design and fabrication technologies for engineering tissues—state of the art and future perspectives. J Biomater Sci Polym Ed 12: 107-124.
12. Annabi N, Tamayol A, Uquillas JA, Akbari M, Bertassoni LE, et al. (2014) 25th Anniversary article: Rational design and applications of hydrogels in regenerative medicine. Advanced Materials 26: 85-124.
13. Schuurman W, Levett PA, Pot MW, van Weeren PR, Dhert WJ, et al. (2013) Gelatin-methacrylamide hydrogels as potential biomaterials for fabrication of tissue-engineered cartilage constructs. Macromolecular Bioscience 13: 551-561.
14. Lewis KJ, Anseth KS (2013) Hydrogel scaffolds to study cell biology in four dimensions. MRS Bull 38: 260-268.
15. Peppas NA, Hilt JZ, Khademhosseini A, Langer R (2006) Hydrogels in biology and medicine: From molecular principles to bio nanotechnology. Advanced Materials 18: 1345-1360.
16. Wu Y, Chen YX, Yan J, Quinn D, Dong P, et al. (2016) Fabrication of conductive gelatin methacrylate-polyaniline hydrogels. Acta Biomater 33: 122-130.
17. Chen YX, Yang S, Yan J, Hsieh MH, Weng L, et al. (2015) A novel suspended hydrogel membrane platform for cell culture. Journal of Nanotechnology in Engineering and Medicine 6: 021002.
18. Thakur NA, DeBoyace SD, Margulies BS (2015) Antagonism of the Met5-enkephalin-opioid growth factor receptor-signaling axis promotes MSC to differentiate into osteoblasts. J Orthop Res 7: 1195-1205.
19. Pradhan S, Chaudhury CS, Lipke EA (2014) Dual-phase, surface tension-based fabrication method for generation of tumor millibeads. Langmuir 30: 3817-3823.
20. Saldaña L, Bensiamar F, Boré A, Vilaboa N (2011) In search of representative models of human bone-forming cells for cytocompatibility studies. Acta Biomater 7: 4210-4221.
21. Ayobian-Markazi N, Fourootan T, Kharazifar MJ (2012) Comparison of cell viability and morphology of a human osteoblastlike cell line (SaOS-2) seeded on various bone substitute materials: An *in vitro* study. DRJ 9: 86-92.
22. Kumar D, Gerges I, Tamplenizza M, Lenardi C, Forsyth NR, et al. (2014) Three-dimensional hypoxic culture of human mesenchymal stem cells encapsulated in a photocurable, biodegradable polymer hydrogel: A potential injectable cellular product for nucleus pulposus regeneration. Acta biomaterialia10: 3463-3474.
23. Chung C, Mesa J, Randolph MA, Yaremchuk M, Burdick JA (2006) Influence of gel properties on neocartilage formation by auricular chondrocytes photoencapsulated in hyaluronic acid networks. Journal of Biomedical Materials Research Part A. 77: 518-525.
24. Li B, Wang L, Xu F, Gang X, Demirci U, et al. (2015) Hydrosoluble, UV-cross-linkable and injectable chitosan for patterned cell-laden microgel and rapid transdermal curing hydrogel *in vivo*. Acta Biomater 22: 59-69.
25. Zhao X, Liu S, Yildirimer L, Zhao H, Ding R, et al. (2016) Injectable stem cell-laden photo cross-linkable microspheres fabricated using microfluidics for rapid generation of osteogenic tissue constructs. Advanced Functional Materials 26: 2809-2819.
26. Visser J, Gawlitta D, Benders KE, Toma SM, Pouran B, et al. (2015) Endochondral bone formation in gelatin methacrylamide hydrogel with embedded cartilage-derived matrix particles. Biomaterials 37: 174-182.
27. Schloßmacher U, Schröder HC, Wang X, Feng Q, Diehl-Seifert B, et al. (2013) Alginate/silica composite hydrogel as a potential morphogenetically active scaffold for three-dimensional tissue engineering. RSC Advances 3: 11185-1194.
28. Wang L, Lu S, Lam J, Kasper FK, Mikos AG (2015) Fabrication of cell-laden macroporous biodegradable hydrogels with tunable porosities and pore sizes. Tissue Eng Part C Methods 21: 263-273.
29. Grigore A, Sarker B, Fabry B, Boccaccini AR, Detsch R (2014) Behavior of encapsulated MG-63 cells in RGD and gelatine-modified alginate hydrogels. Tissue Eng Part A 20: 2140-2150.
30. Yuan Y, Tse KT, Sin FY, Xue B, Fan HH, et al. (2011) *Ex vivo* amplification of human hematopoietic stem and progenitor cells in an alginate three-dimensional culture system. International Journal of Laboratory Hematology 33: 516-525.
31. Chayosumrit M, Tuch B, Sidhu K (2010) Alginate microcapsule for propagation and directed differentiation of hESCs to definitive endoderm. Biomaterials 31: 505-514.